Circulation Research

Locus-Conserved Circular RNA cZNF292 Controls Endothelial Cell Flow Responses

Andreas W. Heumüller, Alisha N. Jones, André Mourão, Marius Klangwart, Chenyue Shi, Ilka Wittig, Ariane Fischer, Marion Muhly-Reinholz, Giulia K. Buchmann, Christoph Dieterich, Michael Potente, Thomas Braun, Phillip Grote, Nicolas Jaé, Michael Sattler, Stefanie Dimmeler

BACKGROUND: Circular RNAs (circRNAs) are generated by back splicing of mostly mRNAs and are gaining increasing attention as a novel class of regulatory RNAs that control various cellular functions. However, their physiological roles and functional conservation in vivo are rarely addressed, given the inherent challenges of their genetic inactivation. Here, we aimed to identify locus conserved circRNAs in mice and humans, which can be genetically deleted due to retained intronic elements not contained in the mRNA host gene to eventually address functional conservation.

METHODS AND RESULTS: Combining published endothelial RNA-sequencing data sets with circRNAs of the circATLAS databank, we identified locus-conserved circRNA retaining intronic elements between mice and humans. CRISPR/Cas9 mediated genetic depletion of the top expressed circRNA cZfp292 resulted in an altered endothelial morphology and aberrant flow alignment in the aorta in vivo. Consistently, depletion of cZNF292 in endothelial cells in vitro abolished laminar flow-induced alterations in cell orientation, paxillin localization and focal adhesion organization. Mechanistically, we identified the protein SDOS (syndesmos) to specifically interact with cZNF292 in endothelial cells by RNA-affinity purification and subsequent mass spectrometry analysis. Silencing of SDOS or its protein binding partner Syndecan-4, or mutation of the SDOS-cZNF292 binding site, prevented laminar flow-induced cytoskeletal reorganization thereby recapitulating cZfp292 knockout phenotypes.

CONCLUSIONS: Together, our data reveal a hitherto unknown role of cZNF292/cZfp292 in endothelial flow responses, which influences endothelial shape.

GRAPHIC ABSTRACT: A graphic abstract is available for this article.

Key Words: cytoskeleton ■ endothelial cells ■ humans ■ mice ■ RNA, circular ■ RNA, non-coding

Endothelial cells play a critical role in the maintenance of organ functions. Being located at the inner wall of the vessels, endothelial cells are exposed to diverse circulating stimuli and blood flow, which itself induces a variety of intracellular signaling cascades.[1,2] Impaired endothelial cell function is associated with various diseases, including atherosclerosis, thrombosis or hypertension, often preceding major vascular events, such as stroke or myocardial infarction. Noncoding RNAs are increasingly recognized as crucial regulators of endothelial cell functions.[3] Circular RNAs (circRNAs) are a subset of noncoding RNAs generated by back splicing of predominantly protein-coding exons. Different from canonical splicing, back splicing ligates a downstream splice donor site with an upstream splice acceptor site, thereby generating covalently closed circRNAs.[4] After the initial identification of various circRNA in endothelial cells,[5] several have been functionally investigated in vitro. For example, cZNF292 (circRNA of ZNF292 [zinc finger protein 292]) silencing was shown to reduce angiogenic responses of cultured endothelial cells in vitro,[5] whereas cHIPK3 silencing prevented retinal vascular dysfunction in diabetes.[6] However,

Novelty and Significance

What Is Known?

- Circular RNA (circRNA) is generated by back splicing of genes and are expressed in high numbers in all tissues.
- CircRNAs have been shown to interact with other RNAs or proteins to regulate cellular function. However, in vivo function is mainly unknown.

What New Information Does This Article Contribute?

- We show that deletion of the circRNA cZfp292 in vivo affects endothelial cell function and morphology, including induction of aberrant flow alignment in the aorta.
- We characterize the mechanism by which the circRNA cZNF292 affects endothelial cell functions showing that cZNF292 interacts with the protein SDOS (syndesmos). This interaction allows endothelial cells to respond to mechanical activation by flow. Inhibition of this interaction by either mutation of the SDOS interaction site or the binding site in cZNF292 blocked the response to laminar flow.
- These findings provide first evidence for the control of flow responses by a circRNA.

In this study, we show that the circRNA cZNF292 interacts with SDOS protein and influences endothelial flow morphology. Mutations interrupting cZNF292-SDOS interactions inhibit laminar flow-induced alignment. This functionality is conserved to the murine circRNA cZfp292, where depletion of cZfp292 leads to aberrant aortic flow alignment in vivo. This novel example of a conserved function of a circRNA/protein interaction in cellular response to mechanical activation highlights the importance of noncoding RNA interactomes in cellular structure and function.

Nonstandard Abbreviations and Acronyms

circRNA	circular RNA
cZNF292	circular RNA of ZNF292
HUVEC	human umbilical vein endothelial cells
PXN	paxillin
SDC4	syndecan-4
SDOS	syndesmos, NUDT16L1
ZNF292/Zfp292	zinc finger protein 292

their mechanism of action is often only poorly understood and evidence for a functional role using genetic ablation models in vivo is rare.[7,8] This is mainly due to the difficulty to eliminate the specific circRNA without altering the levels of the linear host mRNA produced from the same gene. In the case of circRNA Cdr1as, it was possible to delete the entire locus since the linear mRNA was lowly expressed.[7] This deletion was shown to affect brain function.[7] Other studies mutated or deleted flanking regions to reduce circRNA biogenesis[8] or have used short hairpin RNAs to target the back-splice site,[9] however, such approaches often are confounded by off-target effects.

To circumvent these issues and understand the impact of circRNAs in vascular biology in vivo, we aimed to target circRNAs containing intronic sequences as identified in previous studies,[10] with the perception that introns

are not part of the mature mRNA of the host gene, and therefore, can be targeted for selective circRNA deletion.

METHODS

Data Availability

All of the data and information supporting the findings of this study are stated in the article, the Supplemental Material, the Major Resource Table in the Supplemental Material, or are available from the corresponding author upon request. RNA-sequencing data are publicly available at the Gene Expression Omnibus (GEO) repository under the accession GSE107033 and at the ArrayExpress archive under the accession E-MTAB-11171. Mass spectrometry data are publicly available at the PRIDE repository under the accession PXD029794.

RNA Sequencing

Data were either publicly available[5,11] or generated at the European Molecular Biology Laboratory (Heidelberg, Germany) with paired-end 2×75 nucleotide reads. The removal of rRNA was performed with the Ribo-Zero Gold (Epicenter Biotechnologies, Madison, WI; Catalog no. RS-122-2301) or NEBNext rRNA Depletion kit (New England Biolabs, Frankfurt, Germany; Catalog no. E6310L). The data sets (human umbilical vein endothelial cell [HUVEC] RNaseR, human cardiac microvascular endothelial cell/human aortic endothelial cells) were analyzed as described previously.[11]

RNA-Affinity Purification

RNA-affinity purification was performed using native HUVEC lysates obtained after lysis in µL Buffer R (50 mmol/L Tris HCl

pH=8, 50 mmol/L NaCl, 0.5% [v/v] NP-40, 0.1 mmol/L MgCl$_2$, and 1× Protease Inhibitor Cocktail). Lysates were diluted to working concentration of RNase R buffer, and linear RNA was partially degraded by incubation with RNase R for 10 minutes. For pulldown, 1 µL of 100 µmol/L 2′O-Me biotinylated RNA-antisense probes (IDT) were added to the lysates and incubate over night with gently agitation. Probes were recovered using blocked Dynabeads MyOne Streptavidin-Beads C1 beads for 1 hour a t room temperature after which beads were washed and samples were eluted by replacement with D-Biotin. Samples were submitted to 2/3 for analysis by mass spectrometry and 1/3 was used for RNA analysis.

Electrophoretic Mobility Shift Assays

Electrophoretic mobility shift assays were performed using 5 nmol/L ^{32}P-labeled RNA incubated with increasing concentrations of SDOS (syndesmos) protein (wild type or mutant) in buffer containing 10 mmol/L 4-(2-hydroxyethyl)-1-piperazineethanesulfonic acid (HEPES), 100 mmol/L NaCl, and 1 mmol/L beta-mercaptoethanol. Reactions were run on a 0.7% agarose dissolved in 1X TBE. Gels were exposed for 2 hours on a GE-phosphor plate before scanning on a Typhoon 9000 imager. Band intensity was quantified using ImageJ, followed by fitting in Kaleidograph for determination of the dissociation constant with the Hill-equation. Errors indicated represent the error of fit. At least 2 biological replicates were run for each electrophoretic mobility shift assay.

Laminar Flow Experiments

Laminar flow experiments were performed using the Ibidi Perfusion System was used. A total of 2.5×10^5 HUVECs were reseeded 24 hours after siRNA silencing or 48 hours after lentiviral overexpression to 0.4 Luer Ibidi µ-Slides and were allowed to attach for 3 hours. Cells were exposed to unidirectional laminar flow (12 dyn/cm^2, 40 hours) using the Ibidi Perfusion System following the suppliers' instructions. For static controls, cells were not exposed to flow and media was changed daily. Following, cells were washed once with PBS containing calcium and magnesium and fixed with 4% formaldehyde/PBS for 10 minutes at room temperature.

Immunofluorescence Labeling

Immunofluorescence labeling were performed after cells were reseeded 24 hours following siRNA silencing to fibronectin coated 4-well (1×10^5 HUVECs) or 8-well (4×10^4 HUVECs) chamber µ-slides (Ibidi) and cultured for an additional 24 hours. Afterwards, cells were washed once with PBS, fixed with 4% formaldehyde/PBS for 10 minutes at room temperature, permeabilized with 0.1% TritonX-100 for 10 minutes at room temperature, blocked in 10% normal donkey serum and stained with primary antibodies in the blocking solution overnight at 4°C. Antibodies used for staining were as follows: PXN (paxillin; abcam, ab32084, 1:200), Cd144 (BD, no. 555289, 1:50), CD31 (BD, no. 553370, 1:50), ERG (ETS-related gene; abcam, ab92513, 1:200). Cells were washed thrice with PBS containing 0.05% Tween-20 before incubation with fluorescent labeled secondary antibodies (1 hour, room temperature in PBS). F-Actin staining were performed with Phalloidin-488 (ThermoFisher Scientific) and included during the secondary antibody incubation at a dilution

of 1:50. 4′,6-diamidino-2-phenylindole (DAPI) stainings were included during the secondary antibody incubation at a dilution of 1:200. Cells were mounted in Fluoromount-G and imaged using a NikonTie2 Eclipse microscope or Leica SP8 confocal microscope.

Lentiviral Overexpression

Lentiviral overexpression was achieved with virus produced in Lenti-X 293T cells (Takara) using psPAX2 (Addgene, no. 12260) and pMD2.g (Addgene, no. 12259) as packaging vectors and GeneJuice (Merck Milipore, 70967) as transfection reagent following the manufacturers' instructions. Constructs for lentiviral overexpression were cloned from SDOS-Myc expressing vector (Origene, RC202638) into pLenti4V5/DEST Gateway Cloning Vector using SpeI and MluI. Control vector were generated by the same procedure using the empty pCMV6-Entry vector (Origene, PS100001). Viral supernatants were concentrated using the Lenti-X Concentrator (Takara, PT4421-2) and resuspended to match a 40× concentrate. HUVECs were transduced with lentivirus at a final concentration of 1×. Expression was determined experimentally by quantitative polymerase chain reaction to ensure comparable expression of constructs between samples.

Transgenic Mice

Transgenic mice were generated were generated by diploid morula aggregation of knock out transgenic cZfp292 mESC cells as described in Ritter et al.[12] SWISS mice (Janvier) were used as wild-type donor of morula stage embryos and as transgenic recipient host (as foster mothers for transgenic mutant embryos). Offspring was confirmed to be *cZfp292$^{-/-}$* by their fur color agouti and genotyping and backcrossed to C57Bl/6J mice (Janiver). All animal procedures were conducted as approved by local authorities (RP Darmstadt) under the license numbers FU/1064.

Animal Experiments

Animal experiments were performed in accordance with the principles of laboratory animal care as well as according to the German national laws. The studies have been approved by the local ethic committee (Regierungspräsidium Darmstadt, Hessen). For analysis of the aortic endothelium, aortas were dissected, en face prepared and stained according to the protocol published by Ko et al,[13] although fixation was reduced to 2% formaldehyde/PBS for 3 minutes. Animals used for the analysis of the aortic endothelium were between 12 and 20 weeks of age and included animals of both genders. For analysis of retinal blood vessel growth, retinas were prepared from postnatal d7 pups as described previously.[14] All animals were harvested and samples were processed and imaged randomly by personal unaware of the respective genotype.

Statistical Analysis

The ChemiDoc system (Biorad) was used for acquisition of gel and immunoblot data and ImageJ 1.52p was used for image processing. Data were analyzed in Microsoft Excel 2011, GraphPad Prism 5, and Volocity. Data are shown as mean+SEM with individual data points. Data were checked for normality using the Shapiro-Wilk normality test with a threshold of 0.05. *P* values were obtained using Student 2-tailed *t* test or Kolmogorov-Smirnov test and are reported in the figure legends. Multiple-testing

corrections were performed using the Bonferroni-Holm method as stated in the figure legends. Experiments shown in Figure S3E are representative of one experiment. All other data were derived from more biological independent replicates, exact *n* are reported in the figure or the figure legends.

RESULTS

To identify locus-conserved endothelial intronic circRNA, we used published endothelial RNA-sequencing data with circRNAs listed in the circATLAS database (Figure S1A). We first selected circRNAs commonly expressed between different types of human endothelial cells resulting in 1228 circRNAs from 868 host genes (Figure 1A). Further comparison of these circRNAs for their stability towards exonuclease digestion using an additional RNA-sequencing data set of RNase R-treated endothelial cells, showed that 1158 (≈95%) can be considered true circRNA (Figure 1B). However, only 29 of these were back spliced to intronic cassettes (Figure 1C). Importantly, 21 of the
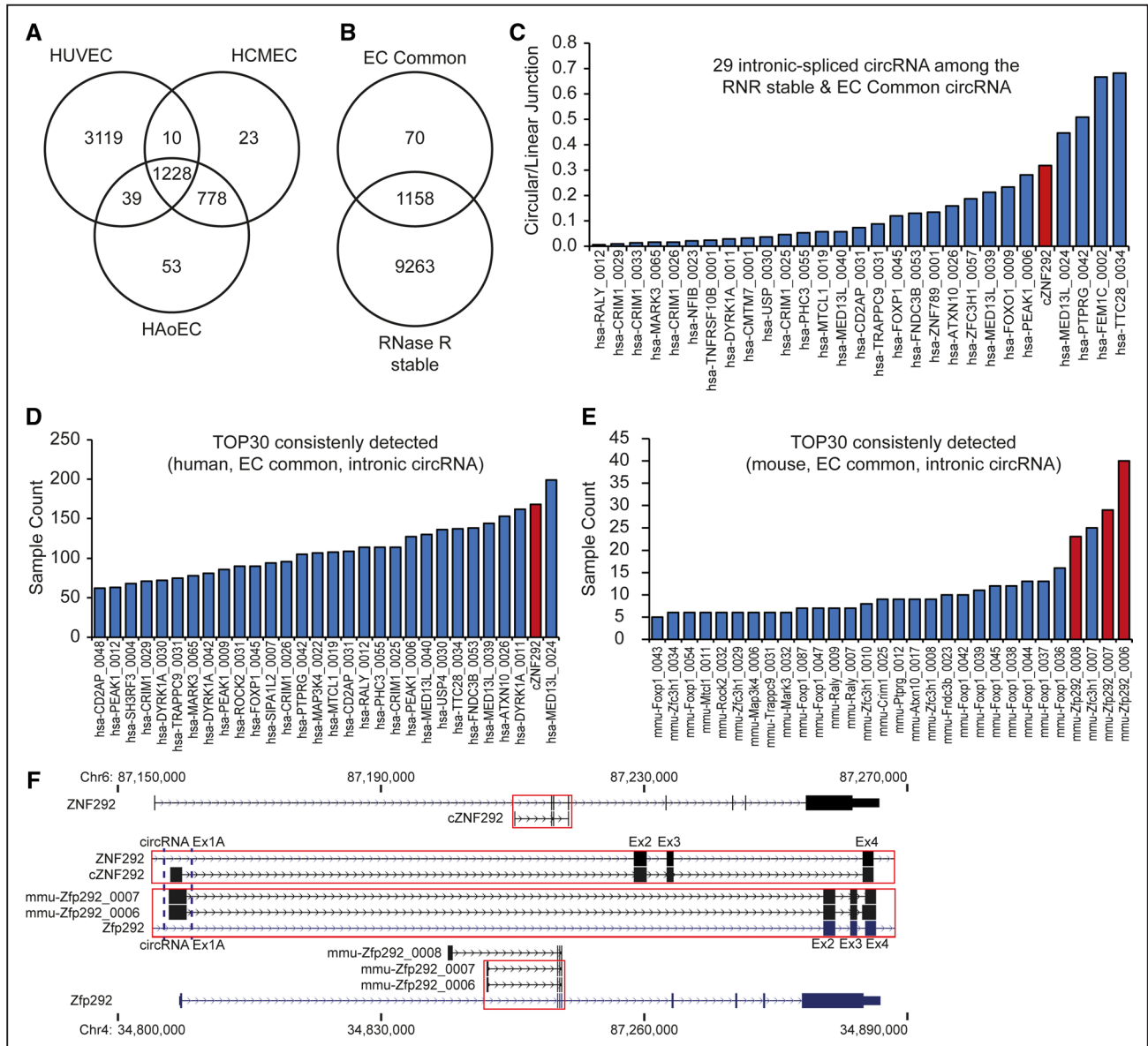
Figure 1. Intron-containing circular RNA (circRNA) screening.
A, Venn diagrams showing commonly expressed circRNAs in different endothelial RNA-sequencing data sets (human umbilical vein endothelial cells [HUVECs], human aortic endothelial cells [HAoECs], and human cardiac microvascular endothelial cells [HCMECs]). The threshold for counting a circRNA as expressed was set to the detection of at least 2 reads in at least 2 samples. **B**, Overlap between endothelial common circRNA and their detection by RNA-seq of exonuclease RNase R-treated HUVEC RNA. **C**, Intronic-spliced circRNA of the selection shown in **A** and **B** ranked by their circular-to-linear expression ratio in HUVECs. **D**, Top 30 of 1404 human intronic circRNAs of the gene subset shown in **C** listed in the circATLAS database and sorted by detection rate. **E**, Top 30 of 302 murine intronic circRNAs of the gene subset shown in **C** mice listed in the circATLAS database and sorted by detection rate. CircRNAs are listed with their circATLAS identifier. **F**, Human and (inverted) mouse ZNF292/Zfp292 (zinc finger protein 292) locus with conserved circRNA isoforms. EC indicates endothelial cell; and RNR, RNase R.

29 candidates were also included in the top 30 consistently detected human intronic circRNAs of the respective loci (Figure 1D) consolidating their presence in human samples. When we additionally analyzed the respective loci in mouse, several intronic circRNAs were commonly detected in circATLAS database (Figure 1E; overlap of 13 host genes when comparing Figure 1D and 1E) but only few circRNAs shared synteny. Of these candidates, we validated the expression and exonuclease resistance of the circRNAs cZNF292 (hsa-ZNF292_0014) and cFOXP1 (hsa-FOXP1_0045), which were both locus-conserved between human and mice (Figure S1B through S1D). Although both were detectable, cZNF292 was expressed at higher levels. Therefore, we chose the highly and commonly expressed *cZNF292* and its locus-conserved mouse orthologue *cZfp292* (mmu-Zfp292_0007; Figure 1F) as the prime candidate for functional validation.

cZNF292 was previously described as hypoxia-inducible circRNA in endothelial cells.[5] Silencing of cZNF292 reduced proliferation and endothelial cell sprouting in culture[5] but the in vivo functions and mechanism of action was unknown.

The mouse orthologue cZfp292 is resistant to exonuclease digestion and also lacks polyadenylation (Figure 2A and 2B). To test whether removal of the retained intronic cassette leads to a loss of cZfp292 without affecting linear *Zfp292* mRNA, we genetically deleted this region in the immortalized murine endothelial cell line H5V using the CRISPR/Cas9 system (Figure 2C). Indeed, cZfp292 was specifically deleted in several independent exon 1A deletion clones (Figure 2D). Therefore, we generated *cZfp292* mutant mice by the same strategy (Figure 2C). As expected, mice harboring this mutation in the germline (Figure 2E) lacked the circular form cZfp292 while the levels of the linear host gene *Zfp292* mRNA and *Zfp292* protein were unaltered (Figure 2F, Figure S2A and S2B). Homozygous mutants were born at the expected Mendelian ratios and no gross abnormalities were observed during postnatal development. Furthermore, when we analyzed angiogenic vascular growth in the postnatal retina of these mice, we did not detect significant perturbations in angiogenic sprouting (Figure 3A and 3B). However, aortic sprout outgrowth was significantly impaired in cZfp292 mutant mice compared with wild-type controls (Figure 3C and 3D). *cZfp292*-deficient endothelial cells from the largest arterial vessel—the thoracic aorta—revealed an altered flow morphology (Figure 3E and 3F, Figure S2C and S2D). Interestingly, RNA-sequencing data and quantitative polymerase chain reaction measurements indicated higher cZNF292 levels in arterial endothelial cells compared with microvascular cells and other cells of the vascular bed (Figure S2F and S2G), which may underlie the observed phenotypic differences.

Next, we aimed to determine whether cZNF292/cZfp292 is involved in flow-sensing and to explore the mechanism how cZNF292 affects cell morphology.
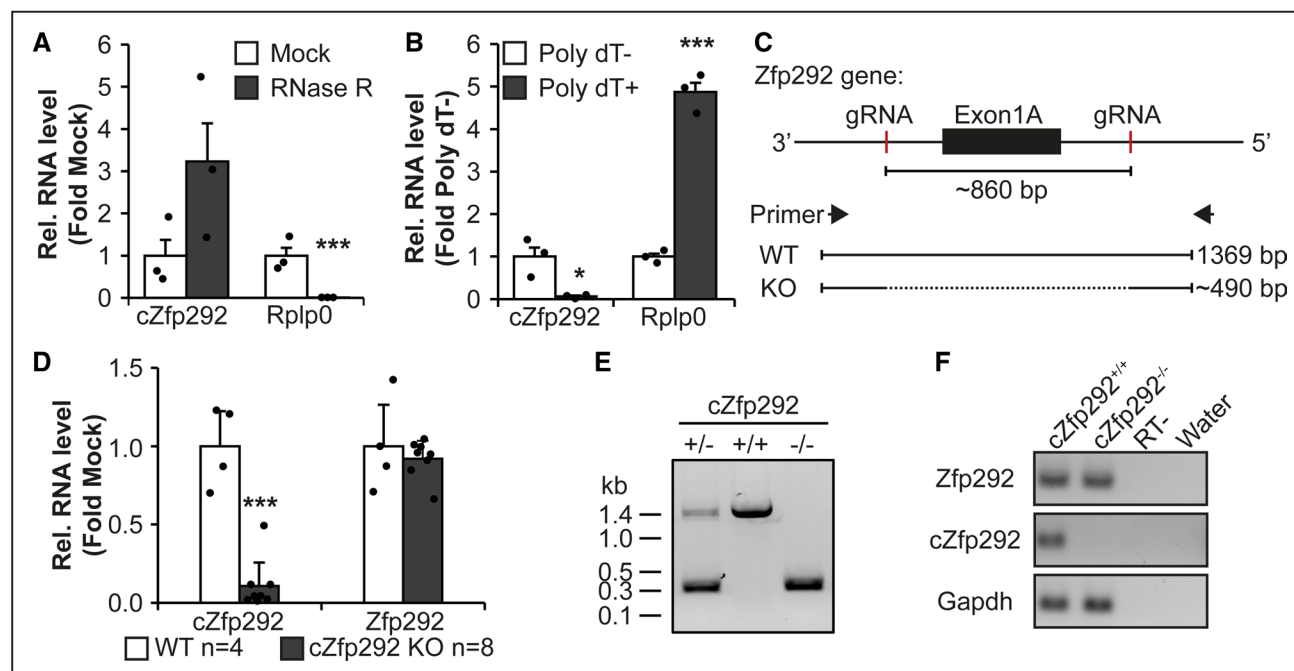

Figure 2. cZfp292 is specifically depletable in vivo.
A, Quantitative real-time polymerase chain reaction (qRT-PCR) measuring RNA levels in human umbilical vein endothelial cell (HUVEC) cell lysates after exonuclease digestion or mock treatment (n=3) or (**B**) following Poly-dT fractionation (n=4) of H5V cells. **C**, Scheme depicting the exon1A knockout (KO) strategy. **D**, qRT-PCR measurements of circular and linear Zfp292 RNA levels after exon1A deletion and clonal propagation in H5V cells. Representative gel images showing deletion of cZfp292 on (**E**) DNA level in tail biopsies and (**F**) RNA level in liver tissue samples of cZfp292 wild-type (WT) or mutant mice. Data are depicted as mean±SEM, statistical analysis by 2-sided unpaired Student *t* test (*) a value of *P*<0.05 is considered significant. gRNA indicates guide RNA.
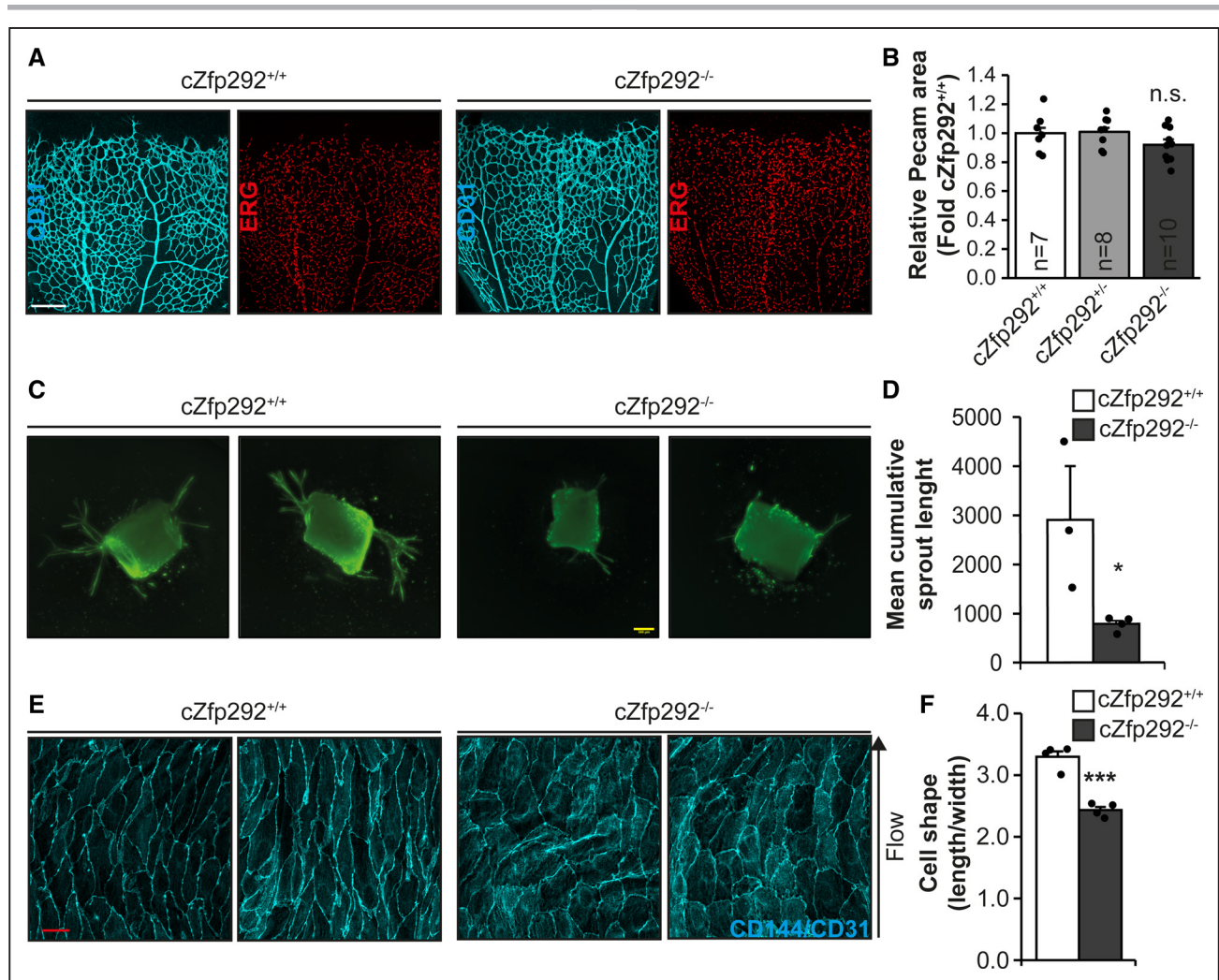
Figure 3. cZfp292 alters endothelial morphology in vivo.

A and **B**, Representative image and quantification of postnatal d7 retina outgrowth in cZfp292⁻/⁻ mice compared with wild-type littermates (samples were stained using the endothelial markers CD31 shown in cyan and ETS-related gene [ERS] shown in red). **C** and **D**, Representative images and quantification of aortic ring sprout outgrowth after 7 d of culture in the presence of 30 ng/mL VEGF-A (vascular endothelial growth factor A). Mean values are representative of 4 technical replicates. **E** and **F**, Images and cell shape quantification of en face stained aorta sections showing endothelial cells (ECs) by CD144 and CD31 staining (n=4). White scale bar equals 200 μm, yellow scale bar equals 100 μm, red scale bar equals 20 μm. Data are depicted as mean±SEM, statistical analysis by 2-sided unpaired Student's t test (*), a value of $P<0.05$ is considered significant.

Since cZNF292 was not detectable in HUVEC high-throughput sequencing of RNA isolated by crosslinking immunoprecipitation data sets and we did not find evidence for translation of these transcripts,[5] we hypothesized that cZNF292/cZfp292 interacts with proteins in endothelial cells. To test this hypothesis, human endothelial cell extracts were treated with or without protease K and protein complexes were separated by size using gradient ultracentrifugation (Figure S3A). Protease treatment shifted cZNF292 to fractions of a lighter weight (Figure S3B and S3C) suggesting that it associates with a protein or a protein complex. To identify the proteins that specifically interact with cZNF292, we performed RNA-affinity purification using antisense oligonucleotides against the exon 1A for pull down, and digested contaminating linear RNA by exonucleases. Using this approach, cZNF292 but not the linear *ZNF292* RNA was enriched (Figure 4A and 4B). Mass spectrometry analysis of the RNA-affinity purifications identified 75 proteins, of which 15 were enriched >10-fold after cZNF292 affinity selection (Figure 4C).

The significantly enriched protein SDOS (also named NUDT16L1) is an RNA-binding protein, known to control focal adhesion signaling and actin cytoskeletal reorganization.[15] SDOS interacts with the cytoplasmic domain of SDC4 (syndecan-4)[15,16] and binds to the focal adhesion adaptor protein PXN.[15,17] Interestingly, Sdc4-deficient mice display poorly aligned endothelial cells in the direction of flow,[18] very similar to what we found in *cZfp292*⁻/⁻ mice. We first verified the interaction of cZNF292 with endogenous SDOS in cZNF292 pulldown samples obtained from HUVEC (Figure 4D) as well as by
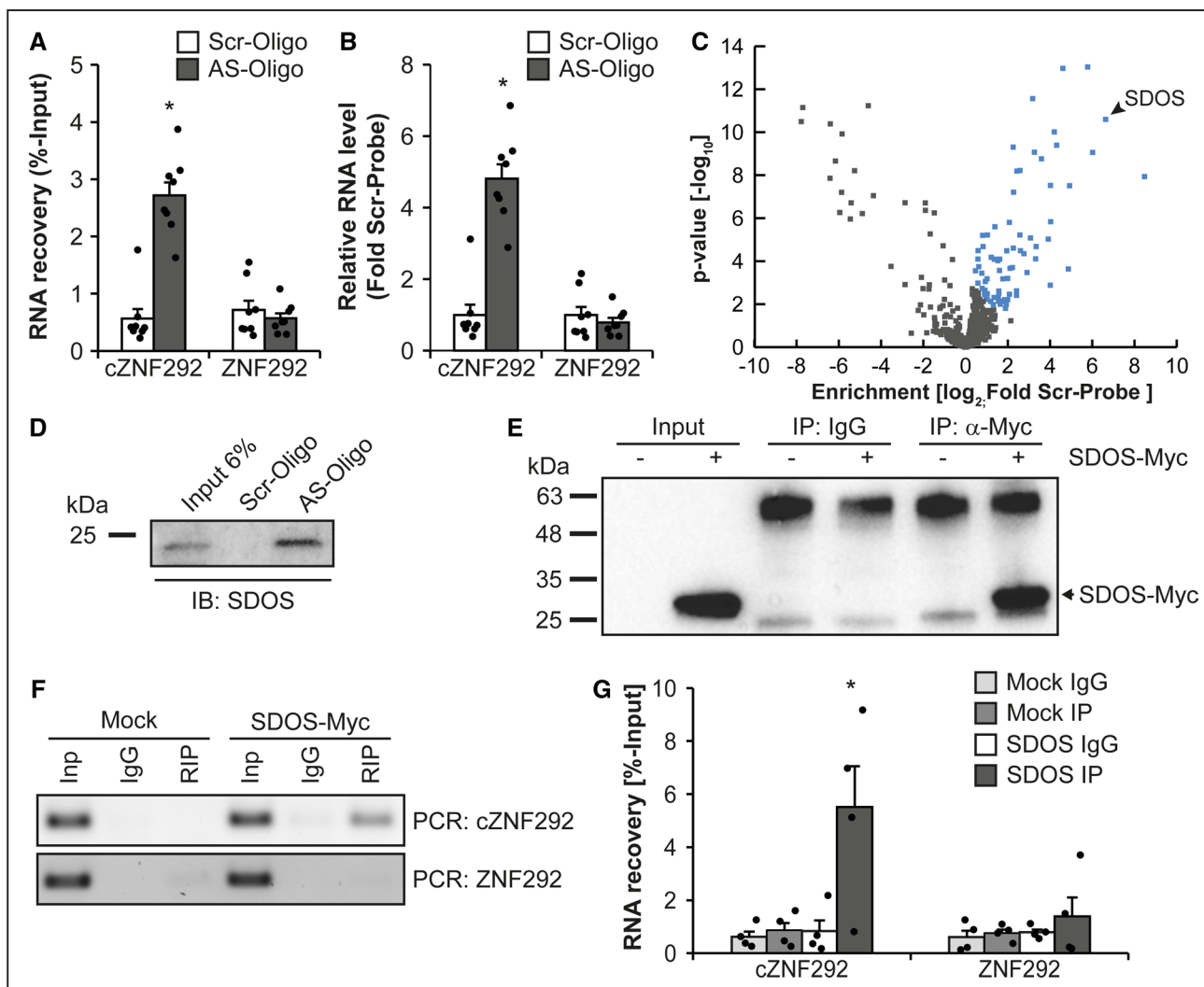
Figure 4. cZNF292 (Circular RNA of ZNF292 [zinc finger protein 292]) interacts with SDOS (syndesmos).
A and **B**, Recovery of circular/linear ZNF292 RNA measured by quantitative real-time polymerase chain reaction (qRT-PCR) after RNA-pulldown using biotinylated-antisense-probes targeting the circular RNA (circRNA) specific exon1A in human umbilical vein endothelial cell (HUVEC) cell lysates under native conditions (n=8). **C**, Volcano plot depicting LC-MS-identified proteins after cZNF292-pulldown in HUVECs (n=8). **D**, Immunoblot showing recovery of endogenous SDOS following native cZNF292-pulldown in HUVEC lysates (n=1). **E**, Representative immunoblot and (**F**) gel images of recovered SDOS-myc and cZNF292 after overexpression of SDOS-myc and immunoprecipitation in HeLa cells, quantification shown in **G** (n=4). Data are depicted as mean±SEM, statistical analysis by 2-sided unpaired Student t test (*) or Kolmogorov-Smirnoff test (#), a value of P<0.05 is considered significant. AS indicates antisense; IgG, immunglobuline G; IP, immunoprecipitation; and Scr, scrambled.

immunoprecipitation showing that Myc-tagged SDOS specifically binds cZNF292/cZfp292 but not the linear host RNA in HeLa cells or H5V cells, respectively (Figure 4E through 4G, Figure S3E). The cZNF292-SDOS interaction was recapitulated with recombinant cZNF292 and purified Myc-tagged SDOS in vitro (Figure S3D and S3F).

To address a functional link between SDC4, SDOS, and cZNF292, we separately silenced the expression of each factor and assessed endothelial cell functions and morphology (Figure S4A). We noticed that 48h post silencing, the typical cobble-stone-like phenotype of cultured endothelial cells started to change and adopt a more activated morphology under static conditions (Figure 5A). These morphological changes were even more striking under conditions of flow (Figure 5A). Here,

endothelial cells lacking cZNF292, SDOS, or SDC4 were resistant to unidirectional flow-induced alignment and reorganization of cytoskeletal filaments and focal adhesion complexes (Figure 5). In detail, silenced endothelial cells did not align in parallel to the direction of flow and showed a random angle of orientation (Figure 5B, Figure S4B through S4D). The flow-induced increase in actin fiber length was significantly reduced by cZNF292, SDOS, or SDC4 silencing (Figure 5A and 5C). Moreover, silenced endothelial cells failed to remodel focal adhesions in response to laminar flow (Figure 5D through 5F). Overall, focal adhesions show a reduction in number but an increase in size in laminar flow-exposed cZNF292, SDOS, or SDC4 silenced endothelial cells compared with scrambled controls (Figure 5E and 5F). Together these
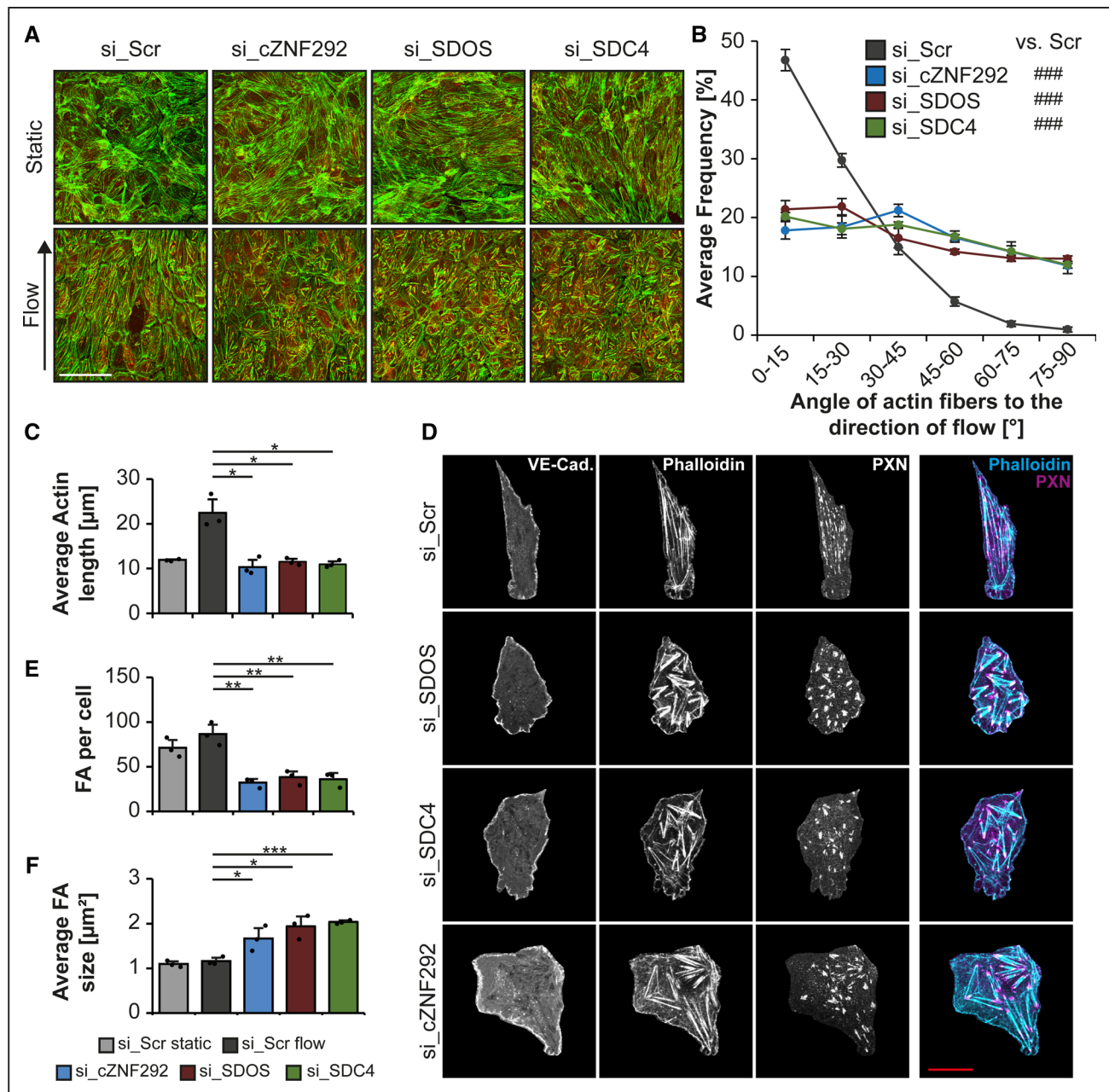
Figure 5. cZNF292 (Circular RNA of ZNF292 [zinc finger protein 292]) and SDOS (syndesmos) silencing prevent cytoskeletal remodeling in response to laminar flow.

A, Representative images of human umbilical vein endothelial cells (HUVECs) after siRNA silencing and exposure to laminar flow stained for actin fibers by phalloidin (green) and the focal adhesion marker PXN (paxillin, shown in red). HUVECs were silenced with siRNA for 24 h before cells were reseeded and exposed to 12 dyne laminar flow for 40 h. Static controls were treated equally but were not exposed to flow. **B**, Distribution of actin fibers compared with the direction of flow in HUVECs following siRNA silencing and laminar flow (n=3). **C**, Quantification of actin fiber length following silencing of cZNF292/SDOS or SDC4 (syndecan-4) and subsequent exposure to flow (n=3). **D**, Single cell excerpts of siRNA silenced HUVECs 40 h after exposure to 12 dyne laminar flow. HUVECs were stained for VE-Cadherin, Actin, and PXN. **E** and **F**, Quantification of focal adhesions (FA) identified by PXN staining in HUVECs following knockdown and laminar flow (in 45 cells of 3 biological replicates). White scale bar equals 100 μm, red scale bar equals 25 μm. Data are depicted as mean±SEM, statistical analysis by 2-sided unpaired Student t test (*) with Bonferroni-Holm correction or Kolmogorov-Smirnoff test (#), a value of $P<0.05$ is considered significant.

data demonstrate that silencing of cZNF292 affects endothelial cell morphology and prevents flow-induced fiber formation and focal adhesions, which is recapitulated by knocking out its binding partner SDOS or the upstream transmembrane proteoglycan SDC4.

To understand the specificity of the circRNA-protein complex, we next determined the sites within cZNF292 that bind to SDOS. A recent study showed that SDOS preferentially binds to C-rich sequences most commonly containing a CCCA/G motif.[19] Both cZNF292

and cZfp292 contain 3 of such putative SDOS binding sites in close proximity to the back-splice site (Figure 6A and 6B). Two of these sites are located in exon 4 and circRNA specific exon 1A contains an additional site. Mouse cZfp292 contains one additional site in exon 1A (Figure 6B). To quantify the interaction strength

between SDOS and cZNF292, we first analyzed the binding capacity of sequences surrounding the back-splice site on exon 4, exon 1A, and exon 4 and the full-length cZNF292 sequence for their binding capacity with recombinant SDOS by electrophoretic mobility shift assays (Figure 6C and 6D). SDOS was bound with
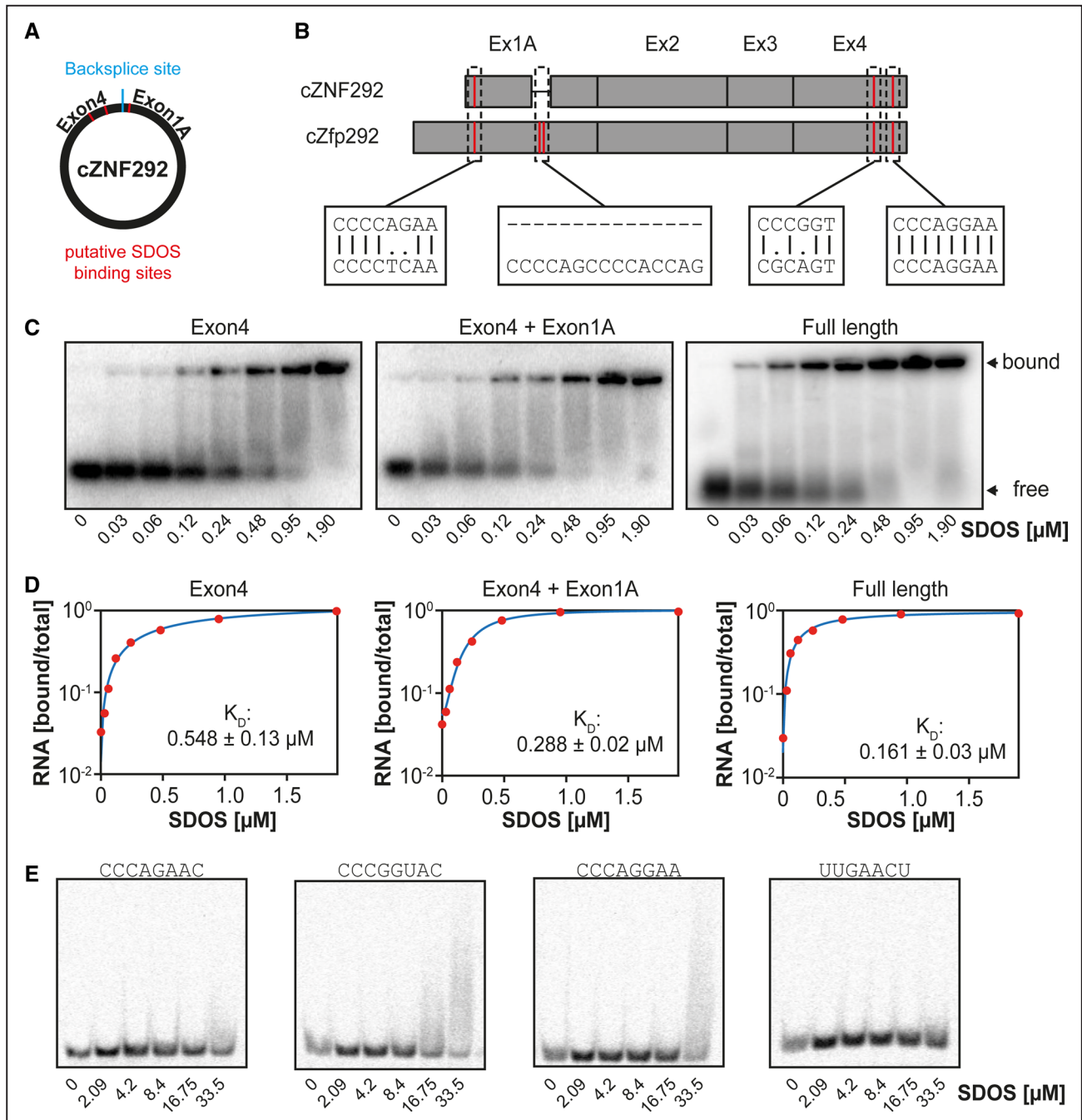
Figure 6. Molecular cZNF292 (circular RNA of ZNF292 [zinc finger protein 292])/SDOS (syndesmos) interaction analysis.
A, Schemes depicting cZNF292 as a circle with potential SDOS binding sites (red) in close proximity to the back-splice site (blue). **B**, Schematic comparison of human and mouse cZNF292/cZfp292 sequence following pairwise sequence alignment and indicating positions of potential SDOS binding sites. **C**, Electrophoretic mobility shift assay (EMSA) depicting interaction between increasing concentrations of SDOS and equal amount of radiolabeled-RNA oligos comprising an excerpt of exon4, exon4+exon1A or the full-length cZNF292 sequence, quantification is shown in **D** (n=2), dissociation constants were calculated using the Hills equation. **E**, Interaction analysis between SDOS and the human SDOS motives outlined in **B** using EMSAs (n=3).

a higher affinity (dissociation constant, K_D: 161 nmol/L) to oligonucleotides covering the full back-spliced region compared with exon 4 alone (K_D: 548 nmol/L) but similar to exon 1A and exon 4 (K_D: 288 nmol/L; Figure 6C). We also validated binding of the predicted sequence motives to SDOS (Figure 6E). Importantly, mutation of the respective motives led to reduced binding between the cZNF292 sequences and SDOS but did not fully prevent the interaction at high SDOS concentrations (Figure S5A). Of note, lentiviral overexpression of cZNF292 with mutated binding sites recapitulated the effects observed by silencing of cZNF292 (Figure S5B through S5F).

Based on these data, we suggest that monomers of the SDOS dimer can bind single motives in the context of the large RNA with multiple binding motifs. Thus, the enhanced affinity resembles avidity compared with individual binding motifs.

To identify the interaction sites in SDOS, we compared the crystal structures of SDOS[16] with published RNA interaction models of its family member NUDT16 and found 4 residues (H29, R55, F66, and E138) that appear critical for RNA binding of SDOS (Figure 7A). Therefore, we mutated the respective residues to alanine and tested the interaction of the mutant with

cZNF292 by RNA immunoprecipitation (Figure 7B and 7C) and electrophoretic mobility shift assay experiments (Figure 7D). Indeed, the SDOS mutants showed a significantly diminished cZNF292 binding activity in both assays (Figure 7B through 7D).

To determine to what extend the interaction of cZNF292 and SDOS contributes to the observed morphological phenotype, we overexpressed a SDOS mutant lacking the cZNF292 interaction sites (Figure 8A, Figure S6A). Lentiviral overexpression of the SDOS 4× Ala mutant but not the wild-type protein prevented flow-induced cell alignments and PXN relocation (Figure 8B through 8D, Figure S6B through S6D) with a very similar phenotype as shown before for silencing of cZNF292 (Figure 5). These data demonstrate that blocking interaction of cZNF292 with SDOS is sufficient to prevent morphological flow responses in endothelial cells.

These results suggest a model whereby cZNF292 enhances SDC4-SDOS interaction and subsequent signaling. To test this model, we determined the effect of cZNF292 overexpression of SDC4-SDOS protein interaction by co-immunoprecipitation. Overexpression of cZNF292 indeed increased the binding of SDC4 to SDOS (Figure 8E and 8F).
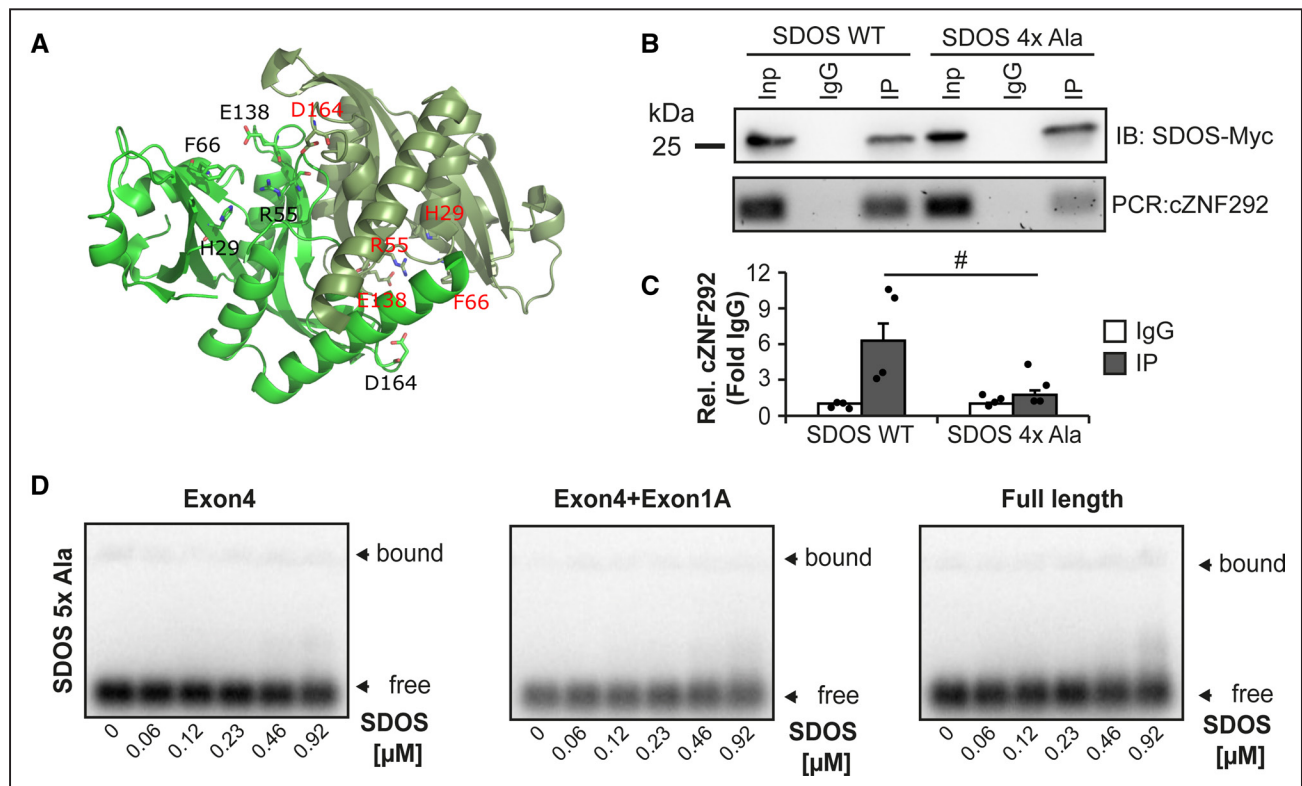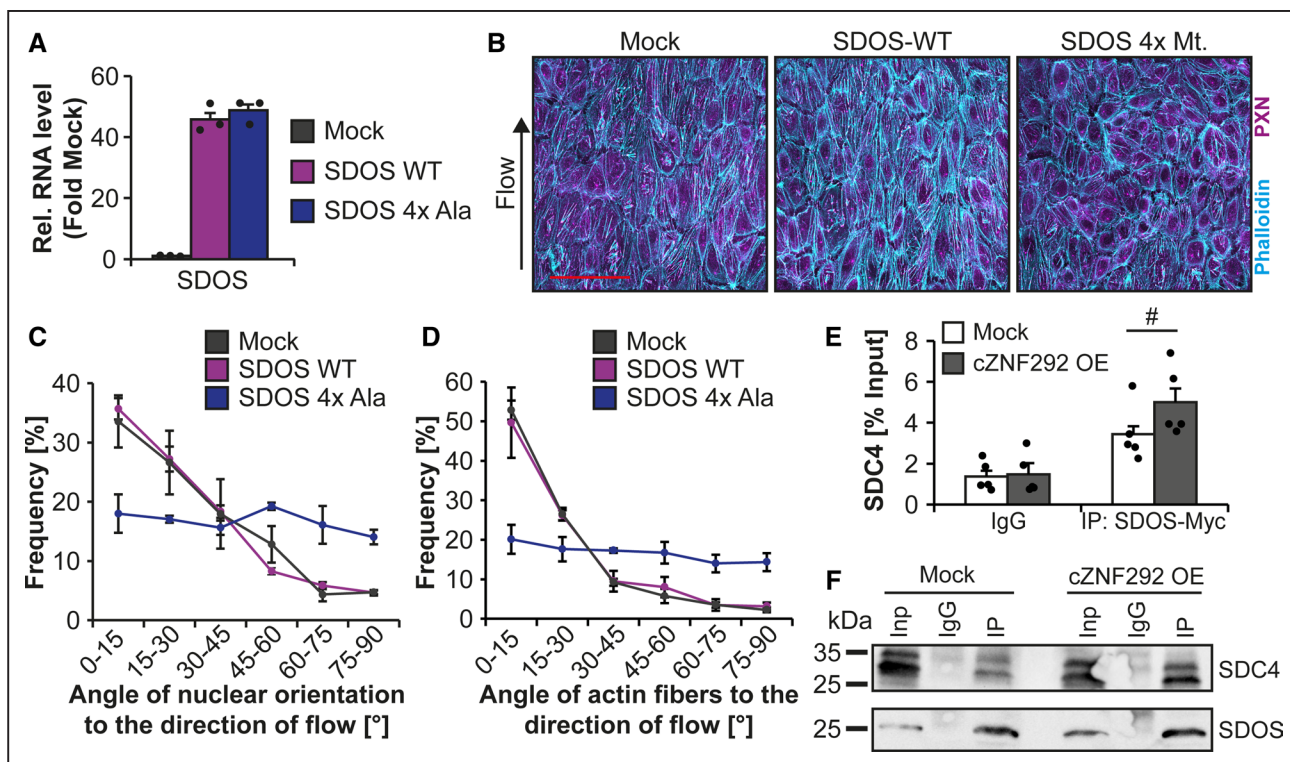

Figure 7. Distinct mutations disrupt cZNF292 (circular RNA of ZNF292 [zinc finger protein 292])/SDOS (syndesmos) interaction.
A, Crystal structure of SDOS (PDB code 3 kvh with symmetry-related molecule representing SDOS dimer) showing predicted RNA-binding residues (red/black by monomer). **B** and **C**, Representative images and quantification of cZNF292 levels after immunoprecipitation of wild-type (WT) or mutated overexpressed SDOS-Myc in HeLa cell lysates (n=5). **D**, Analysis of the interaction between mutated SDOS and RNA oligos comprising the SDOS bindings sites of Exon4, Exon4+Exon1A, or the full-length linear cZNF292 RNA sequence by electromobility shift assay (n=2). IB indicates immunoblot; IgG, immunoglobuline G; Inp, input; IP, immunoprecipitation; and PCR, polymerase chain reaction.

Figure 8. Disruption of cZNF292 (circular RNA of ZNF292 [zinc finger protein 292])/SDOS (syndesmos) interaction alters endothelial flow morphology.
A, Quantification of SDOS RNA levels by quantitative real-time polymerase chain reaction (qRT-PCR) 48 h following lentiviral overexpression of wild-type (WT) and mutated SDOS in human umbilical vein endothelial cells (HUVECs; n=3). **B**, Representative Images of HUVECs following lentiviral overexpression of WT or mutated SDOS and 40 h exposure to 12 dyne laminar flow. HUVECs were stained for actin by phalloidin (cyan) and for the focal adhesion marker PXN (paxillin, shown in magenta). **C**, Distribution of the orientation of nuclei or (**D**) actin fibers compared with the direction of flow in HUVECs after lentiviral overexpression of SDOS variants and exposure to laminar flow (n=2). **E** and **F**, Representative image and quantification of SDC4 (syndecan-4) following immunoprecipitation of SDOS-Myc in HeLa cells (n=5). Membrane-associated fractions were extracted using a commercial kit 48 h after overexpression of SDOS-Myc and SDC4-Flag in the presence of either a cZNF292 overexpression construct (cZNF292 OE) or a respective Mock control. Following SDOS-Myc was precipitated using antibodies targeting the Myc-tag. Immunoblots in **F** were stained for SDC4 (**upper**) and reprobed for SDOS-Myc. Data are depicted as mean±SEM, statistical analysis by 2-sided paired Student t test (#), a value of $P<0.05$ is considered significant. IgG indicates immunoglobuline G; IP, immunoprecipitation; and Inp, input.

CONCLUSIONS

In summary, we show a new approach to determine targetable circRNAs for in vivo characterization and demonstrate that the circRNA cZNF292 interacts with SDOS to regulate endothelial flow responses in vitro and in vivo. It is well established that endothelial cells respond to flow by aligning in the direction of (unidirectional) flow through the reorganization of cytoskeletal filaments and focal adhesion complexes. This crucial adaptive response maintains the anti-inflammatory and atheroprotective properties of the endothelial cell monolayer. Interestingly, we now found that cZNF292/cZfp292 is required for the morphological adaptations of endothelial cells to laminar flow in vitro and in vivo. cZNF292/cZfp292 deficiency thereby recapitulated several known effects of *SDC4* knockouts,[18,20] suggesting that cZNF292/cZfp292 act downstream of SDC4 by influencing the signaling of SDOS and PXN. SDC4 has been proposed as pro-angiogenic molecule in vitro,[21] but physiological

retinal angiogenesis was not disturbed in *Sdc4−/−* mice.[22] Similarly, we previously found cZNF292 silencing to impair angiogenic sprouting in spheroid assays in vitro,[5] whereas cZfp292 deficiency in vivo only resulted in minor alterations of retinal angiogenesis. The difference between the in vitro and in vivo studies may be due to the differences in the multidimensional environment which endothelial cells face. Examples include variances in mechanical forces, which profoundly influence endothelial cell focal adhesions and signaling. Interestingly, we show that outgrowth of aortic endothelial cells, which show highest expression levels of cZNF292 in the vascular bed, was prevented in *cZfp292−/−* mice suggesting that aortic endothelial cells are preferentially affected by the lack of cZfp292. Nevertheless, further studies will need to dissect to which extent the expression of cZfp292 in other cell types contributes to the observed phenotype. Our study is additionally limited by the sole observation of the phenotype under baseline conditions and the unknown function of cZNF292 in humans. It will

be important to assess how cZfp292 may influence the morphology and function of endothelial cells in proatherosclerotic or under other stress conditions.

Our study further demonstrates that cZNF292 directly interacts with SDOS thereby controlling PXN distribution and focal adhesion formation. We have mapped the interaction sites and demonstrate that SDOS binding sites located around the back-splice site are required for the interaction. Importantly, reduction of cZNF292 or mutation of SDOS-cZNF292 interaction sites prevented the morphological adaptation of endothelial cells to flow. Given the known interaction between SDOS with both SDC4[15,16] and PXN,[17] our data, therefore, support a model in which cZNF292 binds to SDOS to comediate SDC4 signaling to PXN, ultimately modulating focal adhesions formation. This model is further supported by the finding that overexpression of cZNF292 augments the interaction of SDOS with SDC4. However, it should be noted that the protein interactions of cZNF292 might not be limited to SDOS given the enrichment of various other proteins following cZNF292 pulldown.

In summary, this study reports that a circRNA acts as a regulator of flow responses in endothelial cells by its interaction with a protein. Only recently, 2 studies reported first insights into the control of endothelial barrier function and adherens junctions by long noncoding RNAs.[23,24] Our study is the first to show a regulatory role of a circRNA, acting as scaffolding component in the fine-tuned cytoskeletal response of endothelial cells to flow.

ARTICLE INFORMATION

Affiliations

Institute of Cardiovascular Regeneration (A.W.H., M.K., A.F., M.M.R., P.G., N.J., S.D.), Faculty for Biological Sciences (A.W.H.), Functional Proteomics, Institute for Cardiovascular Physiology (I.W.), and Institute for Cardiovascular Physiology (G.K.B.), Goethe University, Frankfurt, Germany. Institute of Structural Biology, Helmholtz Zentrum München, Neuherberg, Germany (A.N.J., A.M., M.S.). Biomolecular NMR and Center for Integrated Protein Science Munich at Department Chemie, Technical University of Munich, Garching, Germany (A.N.J., A.M., M.S.). Max Planck Institute for Heart and Lung Research, Bad Nauheim, Germany (C.S., M.P., T.B.). Department of Cardiology, Angiology, and Pneumology, University Hospital Heidelberg, Germany (C.D.). Berlin Institute of Health at Charité − Universitätsmedizin Berlin, Germany (M.P.). Max Delbrück Center for Molecular Medicine in the Helmholtz Association (MDC), Berlin, Germany (M.P.). German Center for Cardiovascular Research (DZHK), Frankfurt, Germany (I.W., M.P., T.B., S.D.). Cardio-Pulmonary Institute (CPI), Frankfurt, Germany (M.P., T.B., S.D.).

Acknowledgments

Author Contributions

Sources of Funding

Disclosures

Supplemental Material

Expanded Material & Methods
Figures S1–S6
References 25–30

REFERENCES

1. Chiu JJ, Chien S. Effects of disturbed flow on vascular endothelium: pathophysiological basis and clinical perspectives. *Physiol Rev.* 2011;91:327–387. doi: 10.1152/physrev.00047.2009

2. Baeyens N, Schwartz MA. Biomechanics of vascular mechanosensation and remodeling. *Mol Biol Cell.* 2016;27:7–11. doi: 10.1091/mbc.E14-11-1522

3. Jaé N, Dimmeler S. Noncoding RNAs in vascular diseases. *Circ Res.* 2020;126:1127–1145. doi: 10.1161/CIRCRESAHA.119.315938

4. Glažar P, Papavasileiou P, Rajewsky N. circBase: a database for circular RNAs. *RNA.* 2014;20:1666–1670. doi: 10.1261/rna.043687.113

5. Boeckel JN, Jaé N, Heumüller AW, Chen W, Boon RA, Stellos K, Zeiher AM, John D, Uchida S, Dimmeler S. Identification and characterization of Hypoxia-regulated endothelial circular RNA. *Circ Res.* 2015;117:884–890. doi: 10.1161/CIRCRESAHA.115.306319

6. Shan K, Liu C, Liu BH, Chen X, Dong R, Liu X, Zhang YY, Liu B, Zhang SJ, Wang JJ, et al. Circular noncoding RNA HIPK3 mediates retinal vascular dysfunction in diabetes mellitus. *Circulation.* 2017;136:1629–1642. doi: 10.1161/CIRCULATIONAHA.117.029004

7. Piwecka M, Glažar P, Hernandez-Miranda LR, Memczak S, Wolf SA, Rybak-Wolf A, Filipchyk A, Klironomos F, Cerda Jara CA, Fenske P, et al. Loss of a mammalian circular RNA locus causes miRNA deregulation and affects brain function. *Science.* 2017;357:eaam8526. doi: 10.1126/science.aam8526

8. Xia P, Wang S, Ye B, Du Y, Li C, Xiong Z, Qu Y, Fan Z. A circular RNA protects dormant hematopoietic stem cells from DNA sensor cGAS-mediated exhaustion. *Immunity.* 2018;48:688–701.e7. doi: 10.1016/j.immuni.2018.03.016

9. Pamudurti NR, Patop IL, Krishnamoorthy A, Ashwal-Fluss R, Bartok O, Kadener S. An in vivo strategy for knockdown of circular RNAs. *Cell Discov.* 2020;6:52. doi: 10.1038/s41421-020-0182-y

10. Zheng Q, Bao C, Guo W, Li S, Chen J, Chen B, Luo Y, Lyu D, Li Y, Shi G, et al. Circular RNA profiling reveals an abundant circHIPK3 that regulates cell growth by sponging multiple miRNAs. *Nat Commun.* 2016;7:11215. doi: 10.1038/ncomms11215

11. Jakobi T, Siede D, Eschenbach J, Heumüller AW, Busch M, Nietsch R, Meder B, Most P, Dimmeler S, Backs J, et al. Deep characterization of circular RNAs from human cardiovascular cell models and cardiac tissue. *Cells.* 2020;9:E1616. doi: 10.3390/cells9071616

12. Ritter N, Ali T, Kopitchinski N, Schuster P, Beisaw A, Hendrix DA, Schulz MH, Müller-McNicoll M, Dimmeler S, Grote P. The lncRNA locus handsdown regulates cardiac gene programs and is essential for early mouse development. *Dev Cell.* 2019;50:644–657.e8. doi: 10.1016/j.devcel.2019.07.013

13. Ko KA, Fujiwara K, Krishnan S, Abe J-I. En face preparation of mouse blood vessels. *J Vis Exp.* 2017;123:55460. doi: 10.3791/55460

14. Lim R, Sugino T, Nolte H, Andrade J, Zimmermann B, Shi C, Doddaballapur A, Ong YT, Wilhelm K, Fasse JWD, et al. Deubiquitinase USP10 regulates Notch signaling in the endothelium. *Science.* 2019;364:188–193. doi: 10.1126/science.aat0778

15. Baciu PC, Saoncella S, Lee SH, Denhez F, Leuthardt D, Goetinck PF. Syndesmos, a protein that interacts with the cytoplasmic domain of syndecan-4, mediates cell spreading and actin cytoskeletal organization. *J Cell Sci.* 2000;113 pt 2:315–324. doi: 10.1242/jcs.113.2.315

16. Kim H, Yoo J, Lee I, Kang YJ, Cho HS, Lee W. Crystal structure of syndesmos and its interaction with Syndecan-4 proteoglycan. *Biochem Biophys Res Commun.* 2015;463:762–767. doi: 10.1016/j.bbrc.2015.06.010

17. Denhez F, Wilcox-Adelman SA, Baciu PC, Saoncella S, Lee S, French B, Neveu W, Goetinck PF. Syndesmos, a syndecan-4 cytoplasmic domain

interactor, binds to the focal adhesion adaptor proteins paxillin and Hic-5. *J Biol Chem*. 2002;277:12270–12274. doi: 10.1074/jbc.M110291200

18. Baeyens N, Mulligan-Kehoe MJ, Corti F, Simon DD, Ross TD, Rhodes JM, Wang TZ, Mejean CO, Simons M, Humphrey J, et al. Syndecan 4 is required for endothelial alignment in flow and atheroprotective signaling. *Proc Natl Acad Sci USA*. 2014;111:17308–17313. doi: 10.1073/pnas.1413725111

19. Avolio R, Järvelin AI, Mohammed S, Agliarulo I, Condelli V, Zoppoli P, Calice G, Sarnataro D, Bechara E, Tartaglia GG, et al. Protein Syndesmos is a novel RNA-binding protein that regulates primary cilia formation. *Nucleic Acids Res*. 2018;46:12067–12086. doi: 10.1093/nar/gky873

20. Vuong TT, Reine TM, Sudworth A, Jenssen TG, Kolset SO. Syndecan-4 is a major syndecan in primary human endothelial cells in vitro, modulated by inflammatory stimuli and involved in wound healing. *J Histochem Cytochem*. 2015;63:280–292. doi: 10.1369/0022155415568995

21. Echtermeyer F, Streit M, Wilcox-Adelman S, Saoncella S, Denhez F, Detmar M, Goetinck P. Delayed wound repair and impaired angiogenesis in mice lacking syndecan-4. *J Clin Invest*. 2001;107:R9–R14. doi: 10.1172/JCI10559

22. Corti F, Wang Y, Rhodes JM, Atri D, Archer-Hartmann S, Zhang J, Zhuang ZW, Chen D, Wang T, Wang Z, et al. N-terminal syndecan-2 domain selectively enhances 6-O heparan sulfate chains sulfation and promotes VEGFA165-dependent neovascularization. *Nat Commun*. 2019;10:1562. doi: 10.1038/s41467-019-09605-z

23. Stanicek L, Lozano-Vidal N, Bink DI, Hooglugt A, Yao W, Wittig I, van Rijssel J, van Buul JD, van Bergen A, Klems A, et al. Long non-coding RNA LASSIE regulates shear stress sensing and endothelial barrier function. *Commun Biol*. 2020;3:265. doi: 10.1038/s42003-020-0987-0

24. Lyu Q, Xu S, Lyu Y, Choi M, Christie CK, Slivano OJ, Rahman A, Jin ZG, Long X, Xu Y, et al. SENCR stabilizes vascular endothelial cell adherens junctions through interaction with CKAP4. *Proc Natl Acad Sci USA*. 2019;116:546–555. doi: 10.1073/pnas.1810729116

25. Rappsilber J, Mann M, Ishihama Y. Protocol for micro-purification, enrichment, pre-fractionation and storage of peptides for proteomics using StageTips. *Nat Protoc*. 2007;2:1896–1906. doi: 10.1038/nprot.2007.261

26. Olsen JV, de Godoy LM, Li G, Macek B, Mortensen P, Pesch R, Makarov A, Lange O, Horning S, Mann M. Parts per million mass accuracy on an Orbitrap mass spectrometer via lock mass injection into a C-trap. *Mol Cell Proteomics*. 2005;4:2010–2021. doi: 10.1074/mcp.T500030-MCP200

27. Cox J, Mann M. MaxQuant enables high peptide identification rates, individualized p.p.b.-range mass accuracies and proteome-wide protein quantification. *Nat Biotechnol*. 2008;26:1367–1372. doi: 10.1038/nbt.1511

28. Tyanova S, Temu T, Sinitcyn P, Carlson A, Hein MY, Geiger T, Mann M, Cox J. The Perseus computational platform for comprehensive analysis of (prote)omics data. *Nat Methods*. 2016;13:731–740. doi: 10.1038/nmeth.3901

29. Trésaugues L, Lundbäck T, Welin M, Flodin S, Nyman T, Silvander C, Gräslund S, Nordlund P. Structural basis for the specificity of human NUDT16 and its regulation by Inosine Monophosphate. *PLoS One*. 2015;10:e0131507. doi: 10.1371/journal.pone.0131507

30. Jost I, Shalamova LA, Gerresheim GK, Niepmann M, Bindereif A, Rossbach O. Functional sequestration of microRNA-122 from Hepatitis C Virus by circular RNA sponges. *RNA Biol*. 2018;15:1032–1039. doi: 10.1080/15476286.2018.1435248